

THz emission from a stacked coherent flux-flow oscillator: non-local radiative boundary conditions and the role of geometrical resonances.

V. M. Krasnov

Department of Physics, Stockholm University, AlbaNova University Center, SE-10691 Stockholm, Sweden
(Dated: May 18, 2010)

I derive simple non-local dynamic boundary conditions, suitable for modelling of radiation emission from stacked Josephson junctions, and employ them for analysis of flux-flow emission from intrinsic Josephson junctions in high- T_c superconductors. It is shown that due to the lack of Lorenz contraction of fluxons in stacked junctions, high quality geometrical resonances are prerequisite for high power emission from the stack. This leads to a dual role of the radiative impedance: on the one hand, small impedance increases the efficiency of emission from the stack, on the other hand, enhanced radiative losses reduce the quality factor of geometrical resonances, which may decrease the total emission power. Therefore, the optimal conditions for the coherent flux-flow oscillator are achieved when radiative losses are comparable to resistive losses inside the stack.

PACS numbers: 74.72.Hs, 74.78.Fk, 74.50.+r, 85.25.Cp

Creation of a compact, high power THz source remains a difficult technological challenge, colloquially known as “the THz gap” [1]. Flux-flow oscillators (FFO’s), based on regular motion of quantized vortices (fluxons) in Josephson junctions, can generate tunable THz radiation with a remarkable linewidth 10^{-12} , albeit with a low emission power $< 1 \mu W$ [2]. The power could be greatly enhanced by coherent phase-locking of several coupled FFO’s [3, 4]. The required coupling is strongest in stacked, atomic scale intrinsic Josephson junctions (IJJs), naturally formed in layered high temperature superconductor $\text{Bi}_2\text{Sr}_2\text{CaCu}_2\text{O}_{8+x}$ (Bi-2212). IJJs allow simple integration of a large number of almost identical stacked Josephson junctions. Furthermore, a large superconducting energy gap in Bi-2212 [5] facilitates operation in the important THz frequency range (up to $\sim 10\text{THz}$). Therefore, IJJs are actively studied both theoretically [6–11] and experimentally [12–17] as possible candidates for realization of a coherent THz oscillator.

Proper radiative boundary conditions are essential for analysis of the coherent FFO. For a single junction this can be done by introducing an appropriate radiation impedance Z [18], connecting *local* ac-components of electric and magnetic fields at the junction edges.

$$Z = Z(\omega) = E_{ac}/H_{ac}. \quad (1)$$

The emission power is $P_{rad} = V_{ac}^2/R_Z$, where $V_{ac} = t_0 E_{ac}$ is the ac-voltage, t_0 is the junction barrier thickness and

$$R_Z = (t_0/w)Z \quad (2)$$

is the radiative resistance of a single junction, w is the width of the junction. However, the stacked FFO can not be described by a single Z because the effective radiative resistance depends not only on the geometry of the stack, but also in a crucial way on the collective fluxon configuration. For example, motion of the triangular fluxon lattice corresponds to $Z \rightarrow \infty$ because it results in out-of-phase oscillations in neighbor junctions $E_i = -E_{i+1}$, leading to destructive interference and negligible emission. On the other hand, motion of the rectangular lattice

corresponds to small Z because it results in in-phase oscillation $E_i = E_{i+1}$, leading to constructive interference and coherent enhancement of the emission power $\propto N^2$, where N is the number of junctions in the stack. Such behavior is caused by the essentially *non-local* nature of magnetic induction [19], which is the consequence of the inductive coupling of junctions in the stack. Therefore, the relation between local E_{ac} and non-local H_{ac} can not be described by Eq. (1).

In this letter I derive simple non-local dynamic radiative boundary conditions for stacked Josephson junctions and employ them for analysis of flux-flow emission from IJJ-based stacked FFO. It is shown that due to the lack of Lorenz contraction of fluxons in stacked junctions [19], high quality $Q \gg 1$ geometrical resonances are prerequisite for high power emission from the stack. This leads to a dual role of the radiative impedance: on the one hand, small Z increases the emission efficiency, but on the other hand, enhanced radiative losses reduce Q of geometrical resonances, which leads to reduction of the emission power. The maximum power is achieved when radiative losses are equal to internal losses in the stack.

Neumann (static) boundary conditions are most widely used for numerical modelling of Josephson junctions:

$$\frac{\partial \varphi}{\partial x}(x=0, L) = B \frac{2\pi \lambda_J \Lambda^*}{\Phi_0}. \quad (3)$$

Here φ is the Josephson phase difference, $x=0, L$ are coordinates of junction edges, B is the applied dc-magnetic field, λ_J is the Josephson penetration depth and Λ^* is the effective magnetic thickness of the junction [19]. As emphasized in Ref. [18], Neumann boundary conditions are non-radiative because they assume $H_{ac}(0, L) = 0$.

Radiative (dynamic) boundary conditions should account for the finite H_{ac} . For a single junction they can be easily written with the help of Eq. (1) [11, 18]:

$$\frac{\partial \varphi}{\partial x}(x=0, L) = \left(B \pm \mu_0 \frac{E_{ac}(0, L)}{Z} \right) \frac{2\pi \lambda_J \Lambda^*}{\Phi_0}. \quad (4)$$

Here plus and minus signs correspond to $x = 0$ and L , respectively, because the direction of emission is opposite at opposite edges of the junction.

However, Eq.(4) is not directly applicable for stacked junctions due to the principle difference in electrodynamics, which is local in single, and non-local in stacked junctions. The electric field E_{ac} is local in each junction because the Debye screening length is always smaller than the electrode thickness d , even for IJJs. However, the magnetic field in inductively coupled stacked junctions is non-local and is created and shared cooperatively by the whole stack [19]. The non-locality of H_{ac} is particularly dramatic for IJJs, for which the London penetration depth $\lambda_{ab} \simeq 200$ nm is much larger than $d < 1$ nm.

To derive the proper non-local radiative boundary conditions for stacked Josephson junctions, let's note that the local relation Eq.(1) is valid outside the stack, however, here the electric field is the result of interference of electric fields from all junctions:

$$E_{ac} = \sum_{i=1}^N E_i. \quad (5)$$

The net emission power from one edge of the stack is

$$P_{rad} = wt_0 H_{ac} \sum_{i=1}^N E_i = wt_0 E_{ac}^2 / Z. \quad (6)$$

Radiative losses are associated with additional currents flowing through edges of the stack:

$$\Delta I_{rad} = w E_{ac} / Z \quad (7)$$

Those displacement-like currents should be added in the numerical scheme for the sake of energy conservation. Equations (4,5,7) together form the final non-local dynamic boundary conditions for stacked Josephson junctions. For the out-of-phase state, $E_i = -E_{i+1}$, $E_{ac} = 0$, they reduce to the non-radiative Neumann condition Eq.(3). For the in-phase state, $E_i = E_{i+1}$, $E_{ac} = N E_i$, they lead to coherent power amplification $\propto N^2$, Eq.(6).

To calculate flux-flow emission, the non-local boundary conditions were implemented into the coupled sine-Gordon equation [4], which describes electrodynamics of inductively coupled stacked Josephson junctions (see Refs.[19, 20] for details of the formalism and the Supplementary [21] for technical details). Simulations were made for $N = 10$ identical IJJs with $L = 4\lambda_J \simeq 2.8$ μm , $w = 1.4$ μm , the stacking periodicity $s = 1.55$ nm, the electrode thickness $d = 0.6$ nm, the ratio of the barrier thickness to the relative dielectric constant $t_0/\epsilon_r \simeq 0.11$ nm, $\lambda_{ab} = 200$ nm, and the critical current density $J_{c0} = 1050$ A/cm². Those parameters correspond to $\lambda_J \simeq 0.7$ μm , the Josephson plasma frequency $\omega_P \simeq 6.4 \times 10^{11}$ 1/s, and the slowest velocity of light $c_N \simeq 3.2 \times 10^5$ m/s, typical for small Bi-2212 mesa structures [17, 22]. The damping parameter $\alpha = (\omega_P R C)^{-1} = 0.05$, corresponds to junction resistance $R \simeq 100$ Ω and the c -axis resistivity $\rho_c \simeq 25$ Ωcm , equal to large bias tunnel resistivity

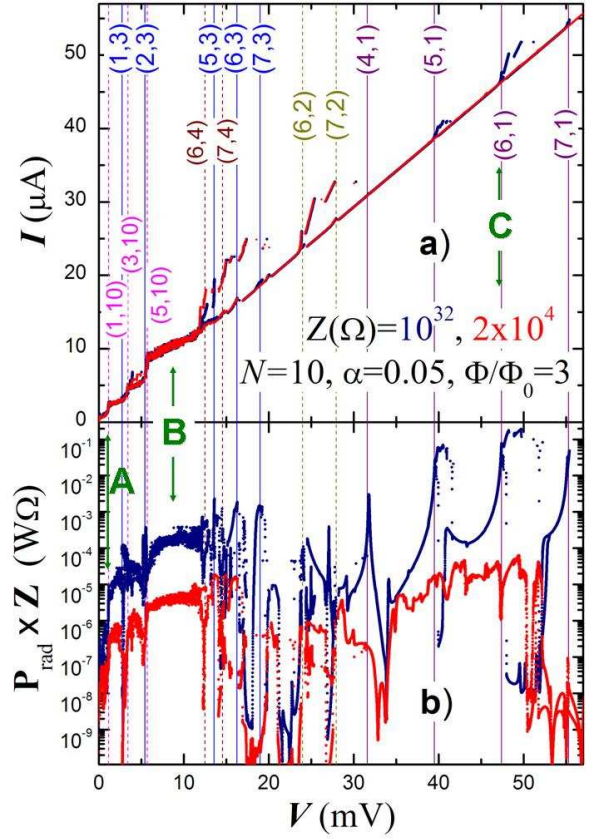


FIG. 1. (color online). Simulated a) $I - V$ characteristics and b) normalized radiative powers for negligible $Z = 10^{32} \Omega$ (dark blue) and moderate $Z = 2 \times 10^4 \Omega$ (red) emission. A variety of Fiske steps is seen. Mode numbers (m, n) for the most prominent steps are indicated. Note that non-radiating even- n steps (dashed vertical lines) are not affected by Z , while radiating odd- n steps (solid lines) vanish for small Z .

of IJJs [23]. However, the quasiparticle (QP) resistivity at small bias and low T can be up to two orders of magnitude larger [24]. Therefore, $\alpha = 0.05$ represents the highest limit of QP damping in IJJs. The correct α is important for numerical modelling because it determines $Q \propto 1/\alpha$ in the absence of radiative losses. Simulations were also performed for smaller α down to 0.005, which show qualitatively similar behavior [17], but require substantially longer integration times. However, for larger $\alpha = 0.1$ the number and amplitudes of accessible geometrical resonances were significantly reduced.

Fig. 1 a) shows simulated $I - V$ characteristics for two impedance values, corresponding to negligible $Z = 10^{32} \Omega$ (dark blue) and moderate $Z = 2 \times 10^4 \Omega$ (red curve) radiation losses, at $\Phi/\Phi_0 = 3$, where $\Phi = BLs$ is the flux per junction. Data for $Z = 10^{32} \Omega$ are similar to simulations with non-radiative Neumann boundary conditions [6, 7, 17]. A large variety of Fiske steps is seen.

Geometrical (Fiske) resonances are caused by resonant excitation of phonon-like collective fluxon lattice vibra-

tions [17] in the flux-flow state. In stacked junctions such fluxon phonons are two-dimensional and are characterized by two wave numbers $k_m = \pi m/L$ ($m = 1, 2, 3, \dots$) in plane, and $q_n = \pi n/Ns$ ($n = 1, 2, \dots, N$) in the c -axis direction [25]. Unlike Josephson plasma waves, fluxon phonons have a linear dispersion relation at low frequencies. Fluxon phonons with the wave number q_n propagate with the in-plane velocity c_n [25]. The slowest, c_N , corresponds to the out-of-phase, $q_N = \pi/s$, and the fastest, c_1 , to the in-phase, $q_1 = \pi/Ns$, mode. Fiske steps occur when the ac-Josephson frequency coincides with the frequency of one of the cavity modes (m, n) [17]:

$$V_{m,n} = \Phi_0 m c_n / 2L, \quad (m = 1, 2, 3, \dots, n = 1, 2, \dots, N). \quad (8)$$

In Fig. 1, voltages of the most prominent phase-locked Fiske steps $NV_{m,n}$ are marked by vertical lines together with mode numbers (m, n) . For the non-radiative case $Z = 10^{32} \Omega$, Fiske steps with both even and odd n are equally represented. However, for $Z = 2 \times 10^4 \Omega$ we observe a clear difference between even and odd n resonances: even- n steps, e.g. (1,10), (3,10), (5,10), (6,4), (7,4), (6,2) and (7,2) are practically the same as for $Z = 10^{32} \Omega$, but all odd- n steps are strongly reduced. For example, steps (5,3), (5,1) and (6,1) are well developed for $Z = 10^{32} \Omega$, but not present for $Z = 2 \times 10^4 \Omega$.

The observed difference between even and odd- n steps for $Z = 2 \times 10^4 \Omega$ is due to appearance of significant radiative losses. For the considered case of even $N = 10$, all even- n resonances are interfering destructively and therefore are non-emitting. To the contrary all odd- n resonances are emitting progressively stronger with decreasing the mode number n . This is most clearly seen from the voltage dependence of the normalized emission power, shown in Fig. 1 b). It can be seen that for $Z = 10^{32} \Omega$ even- n Fiske steps (dashed lines) correspond to minima, while odd- n steps (solid lines) to maxima of emission. As expected, the largest (by two orders of magnitude) emission occurs for in-phase resonances (5,1), (6,1) with the largest Fiske step amplitudes, see Fig. 1 a). They correspond to the velocity matching condition $m \simeq 2 \text{int}[\Phi/\Phi_0]$, as discussed in Ref. [17]. The Fiske step (5,3) has larger amplitude but smaller emission because only one third of the stack is emitting coherently while the rest of the junctions are interfering destructively. Also odd- n Fiske steps (1,3), (3,3), (6,3), (7,3), (4,1), (7,1) with small amplitudes, see Fig. 1 a), produce clear emission peaks for $Z = 10^{32} \Omega$.

Remarkably, all these emission peaks are absent for $Z = 2 \times 10^4 \Omega$. Furthermore, the strongest emission peaks (5,1), (6,1) at $Z = 10^{32} \Omega$ are replaced by minima for $Z = 2 \times 10^4 \Omega$. Apparently, radiative losses have completely damped in-phase resonances for $Z = 2 \times 10^4 \Omega$. This clearly illustrates that the quality factor is playing a central role in operation of the coherent FFO.

The role of the output impedance on the FFO power can be understood from the following simple model. The oscillating amplitude at the resonance is $E_i = E_0 Q = E_0 \omega R_{eff} C$, where E_0 is the amplitude out of the reso-

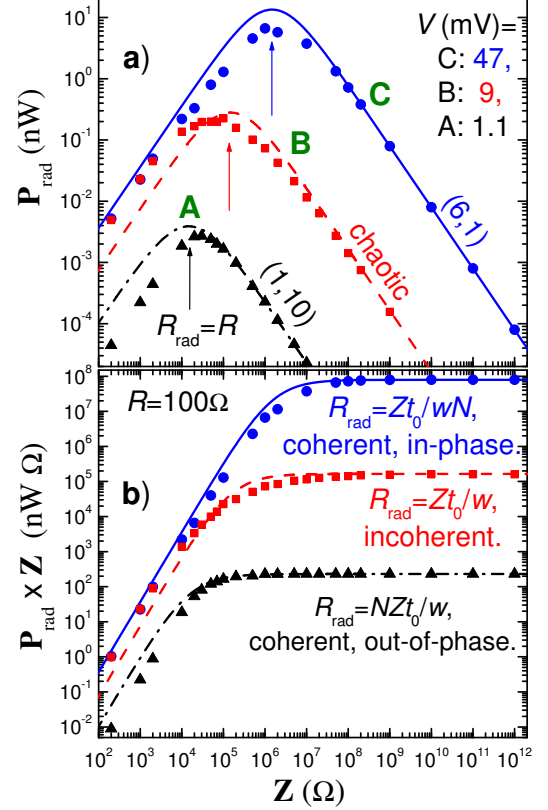


FIG. 2. (color online). Simulated emission characteristics (symbols) as a function of the radiation impedance for three voltages, marked in Fig. 1. A: at the out-of-phase (1,10) resonance, B: in the incoherent state, and C: at the in-phase (6,1) resonance. Lines represent analytic expressions Eqs. (10,11) with R_{rad} indicated in b). It is seen that the emission power is decreasing both at small and large Z and that the maximum power is achieved at $R_{rad} = R$, indicated by arrows in a). Note that the same stack has different values of R_{rad} , depending on collective fluxon dynamics in the stack.

nance and R_{eff} is the effective damping resistance due to both internal QP (R) and radiative (R_{rad}) losses:

$$R_{eff} = [R^{-1} + R_{rad}^{-1}]^{-1}. \quad (9)$$

The total emission power from one side of the junction is

$$P_{rad} = E_0^2 \omega^2 t_0 w \frac{R^2 R_{rad}}{(R + R_{rad})^2}. \quad (10)$$

It is useful to consider the quantity

$$P_{rad} Z = \gamma (1 + R/R_{rad})^{-2}, \quad (11)$$

where γ is constant for a given resonance $\omega_{m,n}$.

As already discussed above, see Eqs. (5,6), radiative losses in stacked Josephson junctions depend essentially on the collective, rather than local, fluxon dynamics. They can be described by the “coherence factor”:

$$C_F = |E_{ac}/E_i|, \quad (12)$$

which reflects the efficiency of emission in comparison to a single junction with the same electric field amplitude. The effective radiative resistance (per junction) is then:

$$R_{rad} = R_Z / C_F. \quad (13)$$

Fig. 2 shows a) the emission power (from one edge) and b) the product $P_{rad}Z$, as a function of Z for three voltage levels, marked by arrows in Fig. 1: A - the coherent, phase-locked state at the lowest out-of-phase geometrical resonance $V_{1,10} \simeq 1.1$ mV; B - an incoherent, chaotic state at $V \simeq 9$ mV at which no clear resonances are observed and individual junctions are having different voltages; C - the coherent in-phase resonance $V_{6,1} \simeq 47$ mV. Symbols and lines represent numerical simulations and analytic expressions, Eqs. (10,11), respectively. It is seen that at large Z , $P_{rad}Z$ is constant. In this case radiative losses are small compared to QP losses, $R_{rad} \gg R$, the amplitude E_{ac} is independent of Z and P_{rad} is increasing $\propto 1/Z$ with decreasing Z , see Eq.(6). However, for $R_{rad} \lesssim R$, the quality factor starts to decrease, resulting in reduction of E_{ac} and the emission power.

According to Eq. (10), the maximum of P_{rad} is achieved when $R_{rad} = R$. However, as follows from Eq. (13), R_{rad} for stacked junctions is not constant, but depends on the collective state of the stack, described by the coherence factor C_F . For the in-phase state C, $C_F = N$ and $R_{rad} = R_Z/N$. The corresponding P_{rad} and $P_{rad}Z$ calculated from Eqs. (10,11) are shown by solid lines in Figs. 2 a) and b) and describe well the numerical data. In this case the maximum of P_{rad} is achieved at large $Z = RNw/t_0$, marked by the blue arrow in Fig. 2 a). The incoherent/chaotic state B, is well described by

Eqs. (10,11) with N -times larger $R_{rad} = R_Z$ (dashed lines), because junctions in the stack act as individual single junctions, $C_F = 1$. Finally, as expected, the out-of-phase state corresponds to the largest R_{rad} which is, however not infinite, but fairly well described by yet another N -times larger $R_{rad} = NR_Z$, $C_F \simeq 1/N$, represented by the dashed-dotted lines.

To conclude, strong emission from the stacked coherent flux-flow oscillator requires both large coherence factor C_F and large oscillating amplitude E_{ac} . For a single junction FFO, E_{ac} can be greatly enhanced due to Lorentz contraction of the fluxon [26] at the velocity matching condition [2]. However, such mechanism is absent in stacked Josephson junctions due to the lack of Lorentz invariance in the system [19]. Therefore, large E_{ac} can be achieved only in the presence of a high quality resonance. Importantly, high quality geometrical resonances can impose their order on the fluxon lattice. E.g., fast in-phase fluxon phonons may stabilize the rectangular fluxon lattice with large $C_F = N$ even at low fluxon velocities [17]. In addition, the resonance reduces the linewidth of emission $\delta f/f \propto 1/Q$. Therefore, high speed geometrical resonances are particularly important for realization of the coherent stacked FFO. As shown above, optimal operation of the coherent FFO is achieved when radiative losses are equal to internal resistive losses. Finally, it was shown that radiative losses lead to the asymmetry between even/odd- n Fiske steps in $I - V$ s of stacked Josephson junctions. This is consistent with recent experimental observations for Bi-2212 mesas [17] and can be viewed as indirect evidence for significant coherent flux-flow emission from intrinsic Josephson junctions.

-
- [1] B. Ferguson and X.C. Zhang, Nature Photonics 1, 26 (2002).
 - [2] V.P. Koshelets and S.V. Shitov, Supercond. Sci. Technol. 13, R53 (2000).
 - [3] P. Barbara, A.B. Cawthorne, S.V. Shitov, and C.V. Lobb, Phys. Rev. Lett. 82, 1963 (1999)
 - [4] S. Sakai, A.V. Ustinov, N. Thyssen and H. Kolstedt, Phys. Rev. B 58, 5777 (1998).
 - [5] V.M. Krasnov, Phys. Rev. B 79, 214510 (2009).
 - [6] R. Kleiner, T. Gaber and G. Hechtfisher, Physica C 362, 29 (2001).
 - [7] M. Machida, T. Koyama, A. Tanaka and M. Tachiki, Physica C 330, 85 (2000).
 - [8] L.N. Bulaevskii and A.E. Koshelev, Phys. Rev. Lett. 99, 057002 (2007).
 - [9] V.M. Krasnov, Phys. Rev. Lett. 103, 227002 (2009).
 - [10] S. Sav'el'ev, V.A. Yampolskii, A.L. Rakhmanov and F. Nori, Rep. Prog. Phys. 73, 026501 (2010).
 - [11] X. Hu and S.Z. Lin, Supercond. Sci. Techn. 23, 053001 (2010).
 - [12] G. Hechtfisher, R. Kleiner, A.V. Ustinov, and P. Müller, Phys. Rev. Lett. 79, 1365 (1997).
 - [13] I.E. Batov et al., Appl. Phys. Lett. 88, 262504 (2006).
 - [14] L. Ozyuzer et al., Science 318, 1291 (2007).
 - [15] M.H. Bae, H.J. Lee, and J.H. Choi, Phys. Rev. Lett. 98, 027002 (2007).
 - [16] H.B. Wang et al., Appl. Phys. Lett. 89, 252506 (2006).
 - [17] S.O. Katterwe, A. Rydh, H. Motzkau and V.M. Krasnov, cond-mat (May 2010) (unpublished).
 - [18] L.N. Bulaevskii and A.E. Koshelev, Phys. Rev. Lett. 97, 267001 (2006).
 - [19] V.M. Krasnov, Phys. Rev. B 63, 064519 (2001).
 - [20] V.M. Krasnov and D. Winkler, Phys. Rev. B 56, 9106 (1997).
 - [21] The variety of collective dynamic states in the stack can be seen from the demo-program provided in the Supplementary: see EPAPS Document No...
 - [22] S.O. Katterwe and V.M. Krasnov, Phys. Rev. B 80, 020502(R) (2009).
 - [23] V.M. Krasnov et. al, Phys. Rev. B 65, 140504(R) (2002).
 - [24] S.O. Katterwe, A. Rydh and V.M. Krasnov, Phys. Rev. Lett. 101, 087003 (2008).
 - [25] R. Kleiner, Phys. Rev. B 50, 6919 (1994).
 - [26] A. Laub, T. Doderer, S.G. Lachenmann and R.P. Huebener, Phys. Rev. Lett. 75, 1372 (1995).